

Corresponding Author: *Nitesh Soni*
Postal Address:
SRF, High Energy Physics Group (Belle Group)
Department of Physics,
Panjab University - Chandigarh - 160014, India
Phone: +91-172-2541741
Fax: +91-172-2783336
Email: *nitesh@puhep.res.in*

Measurement of Branching Fractions for $B \rightarrow \chi_{c1(2)}K(K^*)$ at Belle

Belle Collaboration

N. Soni^{ac}, K. Abe^f, K. Abe^{al}, I. Adachi^f, H. Aihara^{an},
K. Arinstein^a, Y. Asano^{ar}, V. Aulchenko^a, T. Aushevⁱ,
A. M. Bakich^{ai}, E. Barberio^q, I. Bedny^a, U. Bitenc^j, I. Bizjak^j,
S. Blyth^t, A. Bondar^a, M. Bračko^{f,p,j}, T. E. Browder^e,
P. Chang^v, Y. Chao^v, A. Chen^t, K.-F. Chen^v, B. G. Cheon^b,
R. Chistovⁱ, S.-K. Choi^d, Y. Choi^{ah}, A. Chuvikov^{ae},
J. Dalseno^q, M. Danilovⁱ, M. Dash^{as}, L. Y. Dong^g,
S. Eidelman^a, Y. Enari^r, D. Epifanov^a, S. Fratina^j,
N. Gabyshev^a, A. Garmash^{ae}, T. Gershon^f, A. Go^t,
G. Gokhroo^{aj}, B. Golob^{o,j}, A. Gorišek^j, J. Haba^f, T. Hara^{ab},
K. Hayasaka^r, H. Hayashii^s, M. Hazumi^f, L. Hinzⁿ,
T. Hokuue^r, Y. Hoshi^{al}, S. Hou^t, W.-S. Hou^v, T. Iijima^r,
K. Ikado^r, A. Imoto^s, K. Inami^r, A. Ishikawa^f, R. Itoh^f,
J. H. Kang^{at}, J. S. Kang^l, P. Kapusta^w, N. Katayama^f,
T. Kawasaki^y, H. R. Khan^{ao}, H. Kichimi^f, H. J. Kim^m,
S. M. Kim^{ah}, S. Korpar^{p,j}, P. Križan^{o,j}, P. Krokovny^a,
R. Kulasiri^c, C. C. Kuo^t, A. Kuzmin^a, Y.-J. Kwon^{at},
T. Lesiak^w, S.-W. Lin^v, D. Liventsevⁱ, G. Majumder^{aj},
F. Mandl^h, T. Matsumoto^{ap}, Y. Mikami^{am}, W. Mitaroff^h,

K. Miyabayashi^s, H. Miyake^{ab}, H. Miyata^y, Y. Miyazaki^r,
 R. Mizukⁱ, D. Mohapatra^{as}, T. Nagamine^{am}, Z. Natkaniec^w,
 S. Nishida^f, O. Nitoh^{aq}, S. Ogawa^{ak}, T. Ohshima^r, T. Okabe^r,
 S. Okuno^k, S. L. Olsen^e, Y. Onuki^y, W. Ostrowicz^w,
 H. Ozaki^f, P. Pakhlovⁱ, C. W. Park^{ah}, R. Pestotnik^j,
 M. Peters^e, L. E. Piilonen^{as}, A. Poluektov^a, Y. Sakai^f,
 N. Sato^r, T. Schietingerⁿ, O. Schneiderⁿ, M. E. Sevier^q,
 H. Shibuya^{ak}, B. Schwartz^a, V. Sidorov^a, J. B. Singh^{ac},
 A. Somov^c, S. Stanič^l, M. Starič^j, T. Sumiyoshi^{ap}, S. Suzuki^{af},
 S. Y. Suzuki^f, F. Takasaki^f, K. Tamai^f, N. Tamura^y,
 M. Tanaka^f, G. N. Taylor^q, Y. Teramoto^{aa}, X. C. Tian^{ad},
 T. Tsuboyama^f, T. Tsukamoto^f, S. Uehara^f, K. Ueno^v,
 T. Uglovⁱ, S. Uno^f, P. Urquijo^q, G. Varner^e, S. Villaⁿ,
 C. C. Wang^v, C. H. Wang^u, Y. Watanabe^{ao}, E. Won^l,
 Q. L. Xie^g, A. Yamaguchi^{am}, Y. Yamashita^x, M. Yamauchi^f,
 J. Ying^{ad}, Y. Yuan^g, C. C. Zhang^g, L. M. Zhang^{ag},
 Z. P. Zhang^{ag} V. Zhilich^a,

^a*Budker Institute of Nuclear Physics, Novosibirsk, Russia*

^b*Chonnam National University, Kwangju, South Korea*

^c*University of Cincinnati, Cincinnati, OH, USA*

^d*Gyeongsang National University, Chinju, South Korea*

^e*University of Hawaii, Honolulu, HI, USA*

^f*High Energy Accelerator Research Organization (KEK), Tsukuba, Japan*

^g*Institute of High Energy Physics, Chinese Academy of Sciences, Beijing, PR
China*

^h*Institute of High Energy Physics, Vienna, Austria*

ⁱ*Institute for Theoretical and Experimental Physics, Moscow, Russia*

^j*J. Stefan Institute, Ljubljana, Slovenia*

^k*Kanagawa University, Yokohama, Japan*

^l*Korea University, Seoul, South Korea*

^m*Kyungpook National University, Taegu, South Korea*

ⁿ*Swiss Federal Institute of Technology of Lausanne, EPFL, Lausanne, Switzerland*

^o*University of Ljubljana, Ljubljana, Slovenia*

^p*University of Maribor, Maribor, Slovenia*

^q*University of Melbourne, Victoria, Australia*

^r*Nagoya University, Nagoya, Japan*

- ^s*Nara Women's University, Nara, Japan*
- ^t*National Central University, Chung-li, Taiwan*
- ^u*National United University, Miao Li, Taiwan*
- ^v*Department of Physics, National Taiwan University, Taipei, Taiwan*
- ^w*H. Niewodniczanski Institute of Nuclear Physics, Krakow, Poland*
- ^x*Nippon Dental University, Niigata, Japan*
- ^y*Niigata University, Niigata, Japan*
- ^z*Nova Gorica Polytechnic, Nova Gorica, Slovenia*
- ^{aa}*Osaka City University, Osaka, Japan*
- ^{ab}*Osaka University, Osaka, Japan*
- ^{ac}*Panjab University, Chandigarh, India*
- ^{ad}*Peking University, Beijing, PR China*
- ^{ae}*Princeton University, Princeton, NJ, USA*
- ^{af}*Saga University, Saga, Japan*
- ^{ag}*University of Science and Technology of China, Hefei, PR China*
- ^{ah}*Sungkyunkwan University, Suwon, South Korea*
- ^{ai}*University of Sydney, Sydney, NSW, Australia*
- ^{aj}*Tata Institute of Fundamental Research, Bombay, India*
- ^{ak}*Toho University, Funabashi, Japan*
- ^{al}*Tohoku Gakuin University, Tagajo, Japan*
- ^{am}*Tohoku University, Sendai, Japan*
- ^{an}*Department of Physics, University of Tokyo, Tokyo, Japan*
- ^{ao}*Tokyo Institute of Technology, Tokyo, Japan*
- ^{ap}*Tokyo Metropolitan University, Tokyo, Japan*
- ^{aq}*Tokyo University of Agriculture and Technology, Tokyo, Japan*
- ^{ar}*University of Tsukuba, Tsukuba, Japan*
- ^{as}*Virginia Polytechnic Institute and State University, Blacksburg, VA, USA*
- ^{at}*Yonsei University, Seoul, South Korea*

Abstract

We have measured the branching fractions for the exclusive decay modes $B \rightarrow \chi_{c1(2)}K(K^*)$ using a 140 fb^{-1} data sample collected by the Belle detector at the KEKB asymmetric-energy e^+e^- collider. The measured branching fractions for $B^+ \rightarrow \chi_{c1}K^+$, $B^0 \rightarrow \chi_{c1}K^0$, $B^0 \rightarrow \chi_{c1}K^{*0}$ and $B^+ \rightarrow \chi_{c1}K^{*+}$ decay modes are $(4.5 \pm 0.2 \pm 0.5) \times 10^{-4}$, $(3.5 \pm 0.3 \pm 0.5) \times 10^{-4}$, $(3.1 \pm 0.3 \pm 0.7) \times 10^{-4}$ and $(4.1 \pm 0.6 \pm 0.9) \times 10^{-4}$, respectively, where the first error is statistical and the second error is systematic. We do not observe statistically significant signals for the

$B \rightarrow \chi_{c2}K(K^*)$ decay modes and set upper limits at the 90% confidence level. We also study the helicity distribution for $B \rightarrow \chi_{c1}K^*$ decay mode and show that the longitudinal polarization component is dominant.

Keywords: B -meson, Charmonium, Branching Fractions, Polarization

PACS: 13.25.Hw, 11.30.Er

1 Introduction

Decays of B mesons to two-body final states including a charmonium meson have played a crucial role in the observation of CP -violation in the B meson system [1]. These decay modes also provide a sensitive laboratory for studying strong interaction (QCD) effects in a heavy meson system. One widely used approximation to handle QCD effects in heavy meson decays is “factorization”, where it is assumed that participating quarks form hadrons without subsequent transfer of quantum numbers between the hadrons. In the factorization limit, two-body B decays of the type $B \rightarrow \chi_{c0}X$ and $\chi_{c2}X$ are suppressed by angular momentum and vector current conservation [2,3]. Belle and BaBar have reported the observation of exclusive $B^\pm \rightarrow \chi_{c0}K^\pm$ [4,5,6] and the measurement of inclusive $B \rightarrow \chi_{c2}X$ decays [7]. A large $B \rightarrow \chi_{c0}K$ signal yield can be explained by either factorization violation or rescattering of $D_s^{(*)}D^{(*)}$ in the final state [8]². This mechanism also predicts a branching fraction for $B \rightarrow \chi_{c2}K$ comparable to that for $B \rightarrow \chi_{c0}K$. The measurement of new branching fractions of both factorization allowed $B \rightarrow \chi_{c1}K^*$ and factorization inhibited $B \rightarrow \chi_{c2}K^*$ decays provides valuable information for understanding of χ_c production in B meson decay. In this paper, we report a study of exclusive decays $B \rightarrow \chi_{c1(2)}K(K^*)$ for both charged and neutral B mesons, where both χ_{c1} and χ_{c2} are reconstructed from the same final state, $\gamma J/\psi$.

These measurements are based on a 140 fb^{-1} data sample which contains 152 million $B\bar{B}$ pairs, collected with the Belle detector [9] at the KEKB asymmetric-energy e^+e^- (3.5 GeV on 8 GeV) collider [10] operating at the $\Upsilon(4S)$ resonance.

¹ on leave from Nova Gorica Polytechnic, Nova Gorica, Slovenia

² Throughout this paper, when a mode is quoted the inclusion of charge conjugate mode is implied.

2 Belle detector

The Belle detector is a large-solid-angle magnetic spectrometer. Closest to the interaction point is a three-layer silicon vertex detector (SVD), followed by a 50-layer central drift chamber (CDC), an array of aerogel threshold Čerenkov counters (ACC), a barrel-like arrangement of time-of-flight (TOF) scintillation counters, and an electromagnetic calorimeter (ECL) comprised of CsI(Tl) crystals. These subdetectors are located inside a superconducting solenoid coil that provides a 1.5 T magnetic field. An iron flux-return located outside of the coil is instrumented to detect K_L^0 mesons and to identify muons. The detector is described in detail elsewhere [9].

3 Event selection

Events with B -meson candidates are first selected by applying general hadronic event selection criteria. These include a requirement on charged tracks (at least three of them should originate from an event vertex consistent with the interaction region), a requirement on the reconstructed center-of-mass (CM) energy ($E^{CM} > 0.2\sqrt{s}$, where \sqrt{s} is the total CM energy), a requirement on the longitudinal (z -direction) component of the reconstructed CM momentum with respect to the beam direction ($|p_z^{CM}| < 0.5\sqrt{s}/c$) and a requirement on the total ECL energy ($0.1\sqrt{s} < E_{ECL}^{CM} < 0.8\sqrt{s}$) with at least two energy clusters. To suppress continuum background, we also require that the ratio of the second and zeroth Fox-Wolfram moments [11] be less than 0.5. To remove charged particle tracks that are poorly measured or do not come from the interaction region, we require $dz < 5$ cm for all tracks other than those identified as decay daughters of K_S^0 , where dz is the track's closest approach to the interaction point along the beam direction.

4 $\chi_{c1(2)}$ meson candidates

The $\chi_{c1(2)}$ meson states are reconstructed *via* the decay mode $\chi_{c1(2)} \rightarrow \gamma J/\psi$ with $J/\psi \rightarrow \ell^+\ell^-$, where ℓ is muon or electron. For muon tracks, identification is based on track penetration depth and the hit pattern in the KLM system [12]. Electron tracks are identified by a combination of dE/dx from the CDC, E/p (E is the energy deposited in the ECL and p is the momentum measured by the SVD and the CDC) and shower shape in the ECL [13]. In order to recover di-electron events in which one or both electrons have radiated a photon, the four-momenta of all photons within 0.05 radian of the e^+ or e^- directions are included in the invariant mass calculation. The invariant mass

windows are -0.06 (-0.15) $\text{GeV}/c^2 \leq M_{\ell^+\ell^-} - M_{J/\psi} \leq 0.036$ GeV/c^2 to select J/ψ candidates in the $\mu^+\mu^-(e^+e^-)$ channels; these intervals are asymmetric in order to include part of the radiative tails. Vertex- and mass-constrained kinematic fits are then performed for selected J/ψ candidates to improve the momentum resolution. The χ_c states are reconstructed by combining a J/ψ candidate with momentum below 2 GeV/c in the CM frame with all photons of energy greater than 0.060 GeV in the laboratory frame; to suppress π^0 we veto photons that, when combined with another photon in the event, satisfy 0.110 $\text{GeV}/c^2 \leq m_{\gamma\gamma} \leq 0.150$ GeV/c^2 . The $\chi_{c1(2)}$ candidates are selected by requiring the mass difference ($M_{\ell^+\ell^-\gamma} - M_{\ell^+\ell^-}$) to lie between 0.385 GeV/c^2 and 0.431 GeV/c^2 for χ_{c1} and between 0.436 GeV/c^2 and 0.482 GeV/c^2 for χ_{c2} . The mass difference resolutions are 9.6 MeV/c^2 and 12.2 MeV/c^2 at χ_{c1} and χ_{c2} , respectively. Mass-constrained fits are applied to all selected χ_{c1} and χ_{c2} candidates. The ($M_{\ell^+\ell^-\gamma} - M_{\ell^+\ell^-}$) mass distribution is shown in Fig. 1 together with fitted curve [7].

5 K or K^* candidates

The K^{*0} and K^{*+} candidates are reconstructed from four decay modes: $K^{*0} \rightarrow K^+\pi^-$ or $K_S^0\pi^0$, and $K^{*+} \rightarrow K^+\pi^0$ or $K_S^0\pi^+$. The kaon likelihood ratio for a track is defined as $\mathcal{L}(K/\pi) = \mathcal{L}(K)/(\mathcal{L}(K) + \mathcal{L}(\pi))$. Charged kaons are identified by requiring $\mathcal{L}(K/\pi)$ to be greater than 0.6. The kaon and pion likelihoods ($\mathcal{L}(K)$ and $\mathcal{L}(\pi)$) are obtained by combining measurements from the TOF and the CDC (dE/dx) with hit information from the ACC. Tracks which are not identified as either a kaon or a lepton are treated as charged pion candidates. In the reconstruction of the decay mode $B^+ \rightarrow \chi_{c1(2)}K^+$, all well-measured tracks other than the ones from the J/ψ are considered to be kaon candidates. In order to eliminate the systematic error from particle identification and to retain high efficiency, no particle identification cut for kaons is applied. The K_S^0 candidates are reconstructed from pairs of oppositely charged pions. The $\pi^+\pi^-$ pair is required to be displaced from the interaction point (IP) by a minimum transverse distance of 0.22 cm for high momentum (> 1.5 GeV/c) candidates and 0.08 cm for those with momentum less than 1.5 GeV/c . The direction of the pion pair momentum must agree with the direction defined by the IP and the vertex displacement within 0.03 rad for high momentum candidates (> 1.5 GeV/c), within 0.1 rad for candidates having momentum between 1.5 GeV/c to 0.5 GeV/c and within 0.3 rad for the remaining low momentum candidates. The invariant mass of the $\pi^+\pi^-$ pair candidate is required to satisfy 0.482 $\text{GeV}/c^2 \leq M_{\pi^+\pi^-} \leq 0.514$ GeV/c^2 . The π^0 candidates are reconstructed from pairs of photons with energies greater than 0.060 GeV . The π^0 candidates are required to have invariant mass 0.120 $\text{GeV}/c^2 < M_{\gamma\gamma} < 0.150$ GeV/c^2 . A mass-constrained fit is per-

formed to obtain the momentum of the π^0 . To reduce the background from slow pions, we require the π^0 momentum to be greater than 0.2 GeV/c in the CM frame.

6 B meson reconstruction

We reconstruct B mesons by combining a χ_{c1} or χ_{c2} candidate with a charged or neutral $K(K^*)$ candidate. We form two independent kinematic variables: the beam constrained mass $M_{bc} \equiv \sqrt{(E_{\text{beam}}/c^2)^2 - ((\vec{p}_{\chi_{c1(2)}} + \vec{p}_{K(K^*)})/c)^2}$, and $\Delta E \equiv (E_{\chi_{c1(2)}} + E_{K(K^*)}) - E_{\text{beam}}$, where E_{beam} is the beam energy, and $p_{\chi_{c1(2)}}$, $E_{\chi_{c1(2)}}$, $p_{K(K^*)}$ and $E_{K(K^*)}$ are momenta and energies in the CM frame of the χ_c states and the $K(K^*)$ mesons, respectively. The B -meson signal window is defined as $5.27 \text{ GeV}/c^2 \leq M_{bc} \leq 5.29 \text{ GeV}/c^2$ for all channels and the ranges for ΔE are $\pm 0.025 \text{ GeV}$ for $B \rightarrow \chi_{c1(2)}K(K_S^0)$, and $\pm 0.040 \text{ GeV}$ for $B \rightarrow \chi_{c1(2)}K^*(K^+\pi^- \text{ or } K_S^0\pi^+)$. A larger range ($-0.050 \text{ GeV} \leq \Delta E \leq 0.030 \text{ GeV}$) is used for $B \rightarrow \chi_{c1(2)}K^{*+}(K^+\pi^0 \text{ or } K_S^0\pi^0)$ to accommodate the wider ΔE distribution that results from energy leakage in the calorimeter for π^0 modes.

7 Signal yield and background estimation

To study various sources of background, we use 5.5 million $B \rightarrow \psi$ inclusive Monte Carlo events generated using the event generator EvtGen [14] and a GEANT3-based program [15] to simulate the Belle detector response. This Monte Carlo sample contains decays of the type $B \rightarrow k$, where k is a three-body final state, e.g. $\chi_{c1}K\pi$ or $J/\psi K\pi$ etc., or two-body decays, e.g. $J/\psi K$ or $J/\psi K^*$ or $\chi_{c1(2)}K(K^*)$ etc. Based on this Monte Carlo study, the backgrounds for $B \rightarrow \chi_{c1(2)}K(K_S^0)$ decay modes can be categorized as J/ψ inclusive and feed-across backgrounds. The J/ψ inclusive background occurs due to a true J/ψ candidate accidentally combining with an unrelated γ to fake a $\chi_{c1(2)}$. Feed-across background is due to one mode being reconstructed as a different mode because of the similarity in event kinematics. For $B \rightarrow \chi_{c1(2)}K^*$ decay modes, there is an additional background due to non-resonant decays of B mesons, i.e. $B \rightarrow \chi_{c1(2)}K\pi$. Non-resonant background peaks at the same place as signal in the M_{bc} and ΔE distributions, but does not peak in the $K\pi$ -mass distribution. We thus extract the number of signal events from a fit to the M_{bc} distribution for $B \rightarrow \chi_{c1(2)}K(K_S^0)$ decay modes but use the $K\pi$ -mass distribution for $B \rightarrow \chi_{c1(2)}K^*$ decay modes. Each component of background has been estimated separately as discussed below.

The J/ψ inclusive background is modeled by the sidebands in the ($M_{\ell^+\ell^-\gamma} -$

$M_{\ell^+\ell^-}$) mass distribution of data and scaled according to the fitted area of the background under the $\chi_{c1(2)}$ signal region. The sidebands are defined as 0.2 GeV/c² to 0.3 GeV/c² and 0.55 GeV/c² to 0.60 GeV/c² in the ($M_{\ell^+\ell^-} - M_{\ell^+\ell^-}$) mass distribution. This model includes a contribution from the combinatorial $\ell^+\ell^-$ background under the J/ψ peak (“fake J/ψ candidates”), which is not present in the ψ inclusive Monte Carlo sample; this component forms about 5% of the J/ψ inclusive background. As a systematic check, the ψ inclusive Monte Carlo has also been used to model the J/ψ inclusive background and the contribution of the J/ψ inclusive background decays have been obtained by excluding the feed-across and non-resonant background decays in the ψ inclusive Monte Carlo sample. A small difference in the fit between the two models has been included in the systematic error.

For each decay mode $i = 1, \dots, 12$, the feed-across background due to other $\chi_{c1(2)}K(K^*)$ decay modes $j = 1, \dots, 12$ with $j \neq i$ is estimated by taking the appropriate Monte Carlo histograms and normalizing them according to the signal yields observed in the modes j . The total feed-across background for mode i is then fixed in the fit. The fitting procedure for all twelve $\chi_{c1(2)}K(K^*)$ modes is repeated, using the signal yields from the previous iteration as input, until we find a stable result.

The non-resonant background shape is obtained from the ψ inclusive Monte Carlo sample. Due to low statistics and similar shapes of the J/ψ inclusive and non-resonant background, it is not possible to float simultaneously the normalizations of both backgrounds in the fit to data. We have little knowledge about the amount of non-resonant background, so when fitting the $K\pi$ -mass distribution the normalization of the J/ψ inclusive background is fixed, while it is floated for non-resonant background. The contributions from non-resonant background decays have been obtained from the ψ inclusive Monte Carlo sample by excluding the feed-across and J/ψ inclusive background decays.

The M_{bc} distributions for $B \rightarrow \chi_{c1(2)}K(K_S^0)$ decay modes are fitted with a Gaussian to describe the signal region. The width and mean value of the Gaussian are fixed in the fit using Monte Carlo values that are calibrated by the $B^+ \rightarrow \chi_{c1}K^+$ decay mode in data because this mode has the highest statistics among the decay modes considered. The background shapes for the J/ψ inclusive and feed-across backgrounds have been modeled as discussed above. The normalization parameter for the feed-across background histogram is fixed while it is floated for the J/ψ inclusive background histogram. Figure 2 displays the fit to the M_{bc} distributions for the (a) $B^+ \rightarrow \chi_{c1}K^+$, (b) $B^+ \rightarrow \chi_{c2}K^+$, (c) $B^0 \rightarrow \chi_{c1}K_S^0$, and (d) $B^0 \rightarrow \chi_{c2}K_S^0$ decay modes. The signal yields extracted from these distributions are listed in Table 1. For the $B \rightarrow \chi_{c2}K(K_S^0)$ mode, no statistically significant signal is seen. As a check, the signal yields have also been obtained by fitting the ΔE distributions for the $B \rightarrow \chi_{c1(2)}K(K_S^0)$ decay modes and are found to be consistent with the

signal yields obtained from the fits to the M_{bc} distributions.

A relativistic P-wave Breit-Wigner function [16] is used to fit the $K^*(892)$ signal region in the $K\pi$ -mass distributions for the $B \rightarrow \chi_{c1(2)}K^*$ decay modes. For $K^*(892)$, the width and peak position of the P-wave Breit-Wigner function are found to be consistent between data and Monte Carlo in the $B \rightarrow J/\psi K^*(892)$ decay modes [17]; therefore, those parameters are fixed to the PDG values in the fit [18]. The shapes of the J/ψ inclusive, feed-across and non-resonant backgrounds are modeled as explained previously. There may be some structure in the $K_2^*(1430)$ region in the $K\pi$ -mass distributions for the $B \rightarrow \chi_{c1(2)}K^*$ decay modes. To accommodate this possibility, we have included a relativistic D-wave Breit-Wigner function in the fits to the $K\pi$ -mass distributions. The mean and width of the D-wave Breit-Wigner function are fixed to the nominal PDG values. Figure 3 shows the fits to the $K\pi$ -mass distribution for the (a) $B^0 \rightarrow \chi_{c1}K^{*0}(K^+\pi^-)$, (b) $B^0 \rightarrow \chi_{c1}K^{*0}(K_S^0\pi^0)$, (c) $B^+ \rightarrow \chi_{c1}K^{*+}(K^+\pi^0)$, and (d) $B^+ \rightarrow \chi_{c1}K^{*+}(K_S^0\pi^+)$ decay modes. The fits to the $K\pi$ -mass distributions for (a) $B^0 \rightarrow \chi_{c2}K^{*0}(K^+\pi^-)$, (b) $B^0 \rightarrow \chi_{c2}K^{*0}(K_S^0\pi^0)$, (c) $B^+ \rightarrow \chi_{c2}K^{*+}(K^+\pi^0)$, and (d) $B^+ \rightarrow \chi_{c2}K^{*+}(K_S^0\pi^+)$ decay modes are presented in Fig. 4. The signal yields extracted from these distributions are listed in Table 1. For the $B^0 \rightarrow \chi_{c1}K^{*0}(K_S^0\pi^0)$ and $B \rightarrow \chi_{c2}K^*$ decay modes, no statistically significant signals are seen. The signal yields have also been checked by fitting the M_{bc} and ΔE distributions for the $B \rightarrow \chi_{c1(2)}K^*$ decay modes. For the M_{bc} and ΔE distributions a K^* is identified if the absolute difference between the invariant mass of an identified $K\pi$ pair and nominal K^* mass is less than $75 \text{ MeV}/c^2$. The signal yields obtained from the fits to the M_{bc} and ΔE distributions are found to be consistent with the signal yields obtained from the fits to the $K\pi$ -mass distributions.

8 Helicity study for $B \rightarrow \chi_{c1}K^*$ decays

A $P \rightarrow VV$ decay may include three possible polarization amplitudes: two transverse and one longitudinal. The contributions of these amplitudes can be obtained from the helicity distribution of the K^* ($\cos\theta_{K^*}$) where θ_{K^*} is defined as the angle between the K^* momentum and the direction opposite to the B momentum in the K^* rest frame. The transverse polarization amplitudes have a $\sin^2\theta_{K^*}$ dependence while the longitudinal amplitude has a $\cos^2\theta_{K^*}$ dependence. We have analyzed the helicity distributions for different $K\pi$ -mass regions. The efficiency-corrected $\cos\theta_{K^*}$ distribution for the signal region ($0.821 \text{ GeV}/c^2 < M_{K\pi} < 0.971 \text{ GeV}/c^2$) is fitted with the function $f(\cos\theta_{K^*}) = a + 3b\cos^2\theta_{K^*} + 2c\sqrt{3ba}\cos\theta_{K^*}$. The fitted value of c (0.01 ± 0.10) is consistent with zero, which shows that the interference with the scalar amplitude is negligible. The helicity distribution for the background obtained from sideband region ($M_{K\pi} < 0.8 \text{ GeV}/c^2$) is flat except for a peak

in the last bin due to the J/ψ inclusive background (Fig. 5(a)); this distribution is significantly different from the helicity distribution for the signal region as shown in Fig. 5(b). We perform a fit to the efficiency-corrected $\cos\theta_{K^*}$ distributions for the signal and sideband regions with the function $F(\cos\theta_{K^*}) = A + 3B\cos^2\theta_{K^*}$ and obtain $A_{\text{sig}}(A_{\text{sb}})$ and $B_{\text{sig}}(B_{\text{sb}})$ for the K^* signal (sideband) region. With these parameters, the background subtracted net K^* helicity angle distribution is extracted with corresponding parameters A^* and B^* by estimating $A^* = A_{\text{sig}} - SA_{\text{sb}}$ and $B^* = B_{\text{sig}} - SB_{\text{sb}}$, where S is the scale factor to subtract non-resonant $K\pi$ contributions and other backgrounds. Thus, based on A^* and B^* , we obtain the longitudinal polarization of K^* . Using the longitudinal polarization amplitude \mathcal{A}_L and the total amplitude \mathcal{A}_{tot} , the longitudinal polarization parameter is expressed as $\eta = \frac{|\mathcal{A}_L|^2}{|\mathcal{A}_{\text{tot}}|^2}$ which is also expressed in terms of A^* and B^* ; $\eta = \frac{B^* + \frac{A^*}{3}}{A^* + B^*}$. It is also observed that the difference in fit with or without inclusion of the last peaking bin of the $\cos\theta_{K^*}$ distribution for the background region is small and the error assigned to η takes into account this effect. To estimate the systematics due to the background shape uncertainty, we obtain the value of η by using the upper sideband region ($1.1 \text{ GeV}/c^2 < M_{K\pi} < 1.3 \text{ GeV}/c^2$) for a background fit. The difference in values obtained using the two different sideband regions is found to be 4.6%, which is treated as a systematic error. To estimate the influence of a possible interference term ($\cos\theta_{K^*}$) on the polarization parameter value, we perform fits taking the signal events from left and right sides of the K^* peak i.e. ($0.821 \text{ GeV}/c^2 < M_{K\pi} < 0.896 \text{ GeV}/c^2$) and ($0.896 \text{ GeV}/c^2 < M_{K\pi} < 0.971 \text{ GeV}/c^2$). In spite of the observed nonzero values of the scalar interference term in these distributions, the change in longitudinal polarization is found to be within 6.8%, which is taken as a systematic error. These two errors have been combined in quadrature to give a total systematic error of 8.2% on polarization parameter (η). Hence the final value of longitudinal polarization parameter η from this analysis is obtained as $\eta = 0.87 \pm 0.09 \pm 0.07$. From this value of η we conclude that the $B \rightarrow \chi_{c1}K^*$ decay is dominated by longitudinal polarization with a lower limit for the longitudinal polarization of 0.69 at the 90% confidence level. This mode has a larger longitudinal polarization than $B \rightarrow J/\psi K^*$ [17,19].

9 Measurement of branching fractions

The branching fraction for each $B \rightarrow \chi_{c1(2)}K(K^*)$ decay mode is estimated by dividing the observed signal yield by the reconstruction efficiency, the number of $B\bar{B}$ events in the data sample and the daughter branching fractions. We have used the daughter branching fractions published in PDG 2004 [18]. Equal production of neutral and charged B meson pairs in $\Upsilon(4S)$ decay is assumed. Reconstruction efficiencies are estimated by applying the same selection cri-

teria to 20,000 signal Monte Carlo events. The efficiencies for each final state are shown in Table 1. Here, the branching fraction of $K^0 \rightarrow K_S^0 \rightarrow \pi^+\pi^-$ is not included in the efficiency calculation. In the fits to data, the width of the χ_{c2} is constrained to be 10% larger than the width of the χ_{c1} as expected from Monte Carlo simulation and the photon resolution. The effect of this assumption is included in the systematic errors. To calculate upper limits (U.L.), we add the statistical and systematic errors in quadrature, and assume that the combined error behaves as a Gaussian. We then follow the prescription of Feldman and Cousins [20]. The branching fractions are summarized in Table 1. The first errors are statistical and the second errors are systematic. The statistical significance (Σ) of the signal in terms of the number of standard deviations is calculated as $\sqrt{-2\ln(\mathcal{L}_0/\mathcal{L}_{max})}$, where \mathcal{L}_{max} and \mathcal{L}_0 denote the maximum likelihood with the nominal signal yield and with the signal yield fixed at zero, respectively. If a decay mode is reconstructed in two final states, e.g. $B^+ \rightarrow \chi_{c1}K^{*+}(K_S^0\pi^+)$ and $B^+ \rightarrow \chi_{c1}K^{*+}(K^+\pi^0)$, the two branching fraction measurements are averaged, weighted by the statistical and systematic errors. Comparison between our measurement and those at BaBar [21,22] is also shown in Table 3.

10 Systematic uncertainties

Various sources of systematic uncertainty are summarized in Table 2. The uncertainty on the tracking efficiency is estimated to be 1.5% for e and π tracks, and 1.1% for μ and K tracks. The pion tracks from K_S^0 decay are from a displaced vertex and thus have a larger systematic error; we include 2% per track uncertainty for pion tracks from K_S^0 decays. The errors on electron and muon identification are 1.6% and 2.2%, respectively. The kaon identification error is estimated to be 1.9%.

Uncertainties on γ and π^0 reconstruction efficiency are 2% and 4%, respectively. The uncertainty in the K_S^0 selection efficiency is checked by comparing yields for a sample of high momentum $K_S^0 \rightarrow \pi^+\pi^-$ decays before and after applying the K_S^0 selection criteria. The efficiency difference between data and Monte Carlo simulation is less than 1.0%.

All modes have a systematic uncertainty due to $\chi_{c1(2)} \rightarrow \gamma J/\psi$ and $J/\psi \rightarrow \ell^+\ell^-$ branching fractions; the uncertainties for these modes are taken from the PDG [18] and added in quadrature.

The detection efficiency is found to have so small dependence as a function of

decay angles that the integrated interference term among amplitudes with different quantum number of the $K\pi$ -system gets almost cancel. Therefore, this effect on the branching fraction is estimated to be less than 1.3%. However, the integrated amplitudes should be added coherently for the non-resonant $K\pi$ background of the same quantum numbers. To estimate possible systematic errors due to interference between the signal and background, we fit the $K\pi$ -mass distribution to a function which assumes a “coherent” background contribution. We define this function as

$$F(m_{K\pi}) = |\sqrt{N_s}S(m_{K\pi}) + \sqrt{(N_b a_c)}e^{i\phi}B_g(m_{K\pi})|^2 + N_b(1 - a_c)B_g^2(m_{K\pi}) \quad (1)$$

where

$$S(m_{K\pi}) = \frac{m_{K^*}\Gamma(m_{K\pi})}{(m_{K\pi}^2 - m_{K^*}^2) + im_{K^*}\Gamma(m_{K\pi})} \quad (2)$$

is a relativistic P-wave Breit-Wigner function with $m_{K^*} = 892 \text{ MeV}/c^2$, $B_g(m_{K\pi})$ is the phase space background function, N_s and N_b are the numbers of events for signal and background, respectively, and a_c is the fraction of coherent background with a varied phase ϕ relative to the signal. The maximum value of the coherent background fraction is taken from the helicity analysis to be $a_c = 0.6$. By varying the phase and relative fraction of coherent background within error in this fit, we find that the maximum difference in the signal yield due to the possible interference term is 15%. This difference is included as a systematic error and listed as “Inter.” in Table 2. We assume that this difference is same for all K^* channels; it is determined from the highest statistics $B \rightarrow \chi_{c1}K^*$ mode.

In this study we have assumed that the background shape is described by the phase space function. We also fit the same distribution by using different background shapes. In one set of fits, a threshold function [17] is used to describe the background shape and in another set the function $B_g(m_{K\pi})(a_1 + a_2P_K + a_3P_{\chi_{c1}})$ is used to describe the background shape; here $B_g(m_{K\pi})$ is the phase space background function, a_1 , a_2 , a_3 are the free parameters in the fit, P_K is the momentum of K in the K^* rest frame and $P_{\chi_{c1}}$ is the χ_{c1} momentum in the B rest frame. The maximum difference in the signal yield obtained by using different background shapes is found to be 10.8% and is taken as an additional systematic error listed as background shape (“Bkg. Shape”) in Table 2. This difference is also determined from the highest statistics $B \rightarrow \chi_{c1}K^*$ mode and assumed to be the same for all K^* modes.

The detection efficiency can depend on the various values of polarization amplitudes for $B \rightarrow \chi_{c1(2)}K^*$ decay modes. To check this effect, the exclusive Monte Carlo sample of $B \rightarrow \chi_{c1}K^*(K^+\pi^-)$ decay with various values of the polarization amplitudes is generated. The maximum difference in detection efficiency is estimated to be 5.1% and treated as systematic error. This differ-

ence is assumed to be the same for all K^* modes.

The yield measurements are taken from fits where the mean and width of the signal shape are fixed. The corresponding uncertainty is estimated by varying the means and widths in turn by $\pm 1\sigma$, and repeating the fit. The percentage change in the signal yield is presented in Table 2. The difference between two background fitting models (i.e. using the J/ψ inclusive background shapes from data or from the ψ inclusive Monte Carlo) has also been included as a systematic error listed as background error (“Bkg. Error”) in Table 2.

For the χ_{c1} mode, the error on the efficiency correction due to the χ_{c1} width is based on the uncertainty of the fitted width in data. For the χ_{c2} mode, there are additional effects due to the assumptions in the fit: $\sigma(\chi_{c2}) : \sigma(\chi_{c1}) = 1.1 : 1$ (estimated in an alternative fit where the χ_{c1} and χ_{c2} widths float independently) and the uncertainty on the correction factor for the feed-across from χ_{c1} . The resulting error estimates are combined in quadrature, and listed as an efficiency correction (“Eff. Corr.”) in Table 2.

The uncertainty on the number of $B\bar{B}$ events, which is common to all modes, is 1%; this is negligible compared to the other systematic errors.

11 Conclusion

We have measured the branching fractions for the $B \rightarrow \chi_{c1(2)}K(K^*)$ decay modes using 152 million $B\bar{B}$ events. Although inclusive χ_{c2} signals in B decay have been observed before [7], we do not find any significant signals for the exclusive two-body $B \rightarrow \chi_{c2}K(K^*)$ decay modes and set upper limits on the branching fractions at the 90% confidence level which are an order of magnitude smaller than those for $B \rightarrow \chi_{c1}K(K^*)$. The helicity distribution for the $B \rightarrow \chi_{c1}K^*$ decay mode shows that the longitudinal polarization component is dominant.

12 Acknowledgments

We thank the KEKB group for the excellent operation of the accelerator, the KEK cryogenics group for the efficient operation of the solenoid, and the KEK computer group and the National Institute of Informatics for valuable computing and Super-SINET network support. We acknowledge support from the Ministry of Education, Culture, Sports, Science, and Technology of Japan and the Japan Society for the Promotion of Science; the Australian Research

Council and the Australian Department of Education, Science and Training; the National Science Foundation of China under contract No. 10175071; the Department of Science and Technology of India; the BK21 program of the Ministry of Education of Korea and the CHEP SRC program of the Korea Science and Engineering Foundation; the Polish State Committee for Scientific Research under contract No. 2P03B 01324; the Ministry of Science and Technology of the Russian Federation; the Ministry of Higher Education, Science and Technology of the Republic of Slovenia; the Swiss National Science Foundation; the National Science Council and the Ministry of Education of Taiwan; and the U.S. Department of Energy.

References

- [1] K. Abe *et al.* (Belle Collaboration), Phys. Rev. Lett. **86**, 2509 (2001); **87**, 091802 (2001); Phys. Rev. D **66**, 071102(R) (2002); **66**, 032007 (2002); B. Aubert *et al.*, (BaBar Collaboration) Phys. Rev. Lett. **86**, 2515 (2001); **87**, 091801 (2001); Phys. Rev. D **66**, 032003 (2002); Phys. Rev. Lett. **89**, 201802 (2002).
- [2] M. Suzuki, Phys. Rev. D **66**, 037503 (2002).
- [3] M. Bauer, B. Stech, M. Wirbel, Z. Phys. C **34**, 103 (1987).
- [4] K.Abe, *et al.* (Belle Collaboration), Phys. Rev. Lett. **88**, 031802 (2002).
- [5] B. Aubert, *et al.* (BaBar Collaboration), Phys. Rev. D **69**, 071103 (2004).
- [6] K.Abe, *et al.* (Belle Collaboration), Phys. Rev. D **71**, 092003 (2005).
- [7] K.Abe, *et al.* (Belle Collaboration), Phys. Rev. Lett. **89**, 011803 (2002).
- [8] P. Colangelo, F.De Fazio and T.N. Pham, Phys. Lett. B **542**, 71 (2002).
- [9] A. Abashian *et al.* (Belle Collaboration), Nucl. Instr. and Meth. A **479**, 117 (2002).
- [10] S. Kurokawa and E. Kikutani, Nucl. Instr. and Meth. A **499**, 1 (2003).
- [11] G. Fox and S. Wolfram, Phys. Rev. Lett., **41** 1581 (1978).
- [12] A. Abashian *et al.*, Nucl. Instrum. Methods Phys. Res., Sect. A **491** 69 (2002).
- [13] K. Hanagaki *et al.*, Nucl. Instrum. Methods Phys. Res., Sect. A **485** 490 (2002).
- [14] We use the EvtGen *B*-meson decay generator developed by the CLEO and the BaBar Collaborations, see: <http://www.slac.stanford.edu/~lange/EvtGen/>.
- [15] CERN program library long writeup W5013, CERN, (1993).
- [16] J. Pisut and M. Roos, Nucl. Phys. B **6**, 325 (1968).
- [17] K. Abe *et al.*, (Belle Collaboration), Phys. Lett. B **538**, 11 (2002).

- [18] S. Eidelman *et al.*, (Particle Data Group), Phys. Lett. B **592**, 1 (2004).
- [19] B. Aubert *et al.*, (BaBar Collaboration), Phys. Rev. Lett. **87**, 241801 (2001).
- [20] G.J. Feldman and R.D. Cousins, Phys. Rev. D **57**, 3873 (1998).
- [21] B. Aubert *et al.*, (BaBar Collaboration), Phys. Rev. Lett. **94**, 171801 (2005).
- [22] B. Aubert *et al.*, (BaBar Collaboration), Phys. Rev. Lett. **94**, 141801 (2005).

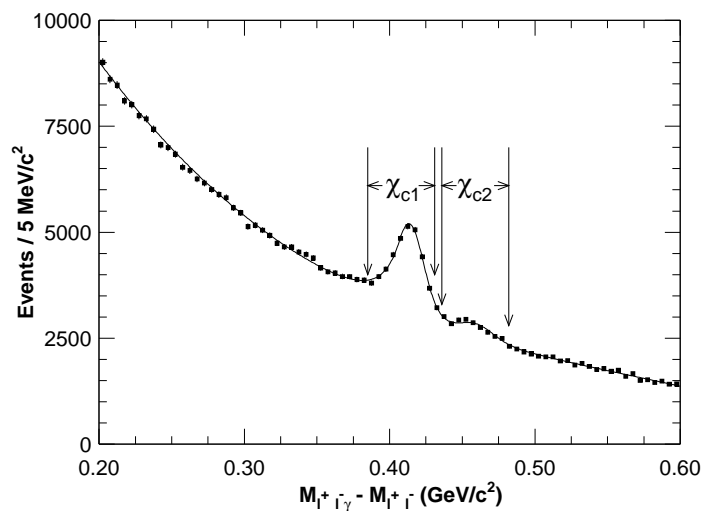


Fig. 1. The $(M_{\ell^+\ell^-\gamma} - M_{\ell^+\ell^-})$ mass difference distribution with the selected χ_{c1} and χ_{c2} mass regions.

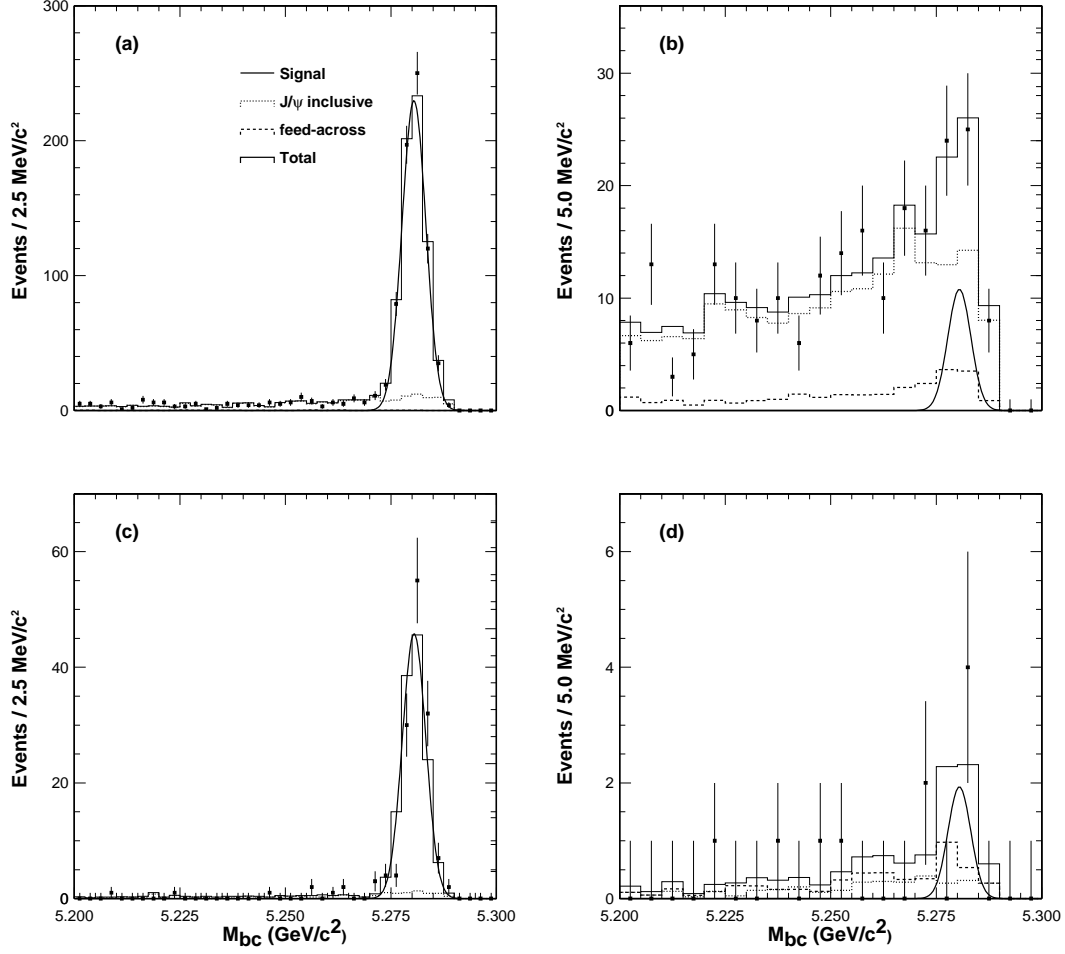


Fig. 2. The M_{bc} distribution for (a) $B^+ \rightarrow \chi_{c1}K^+$, (b) $B^+ \rightarrow \chi_{c2}K^+$, (c) $B^0 \rightarrow \chi_{c1}K_S^0$ and (d) $B^0 \rightarrow \chi_{c2}K_S^0$ decay modes, respectively, together with results of the fit for the signal region and contributions due to J/ψ inclusive and feed-across backgrounds.

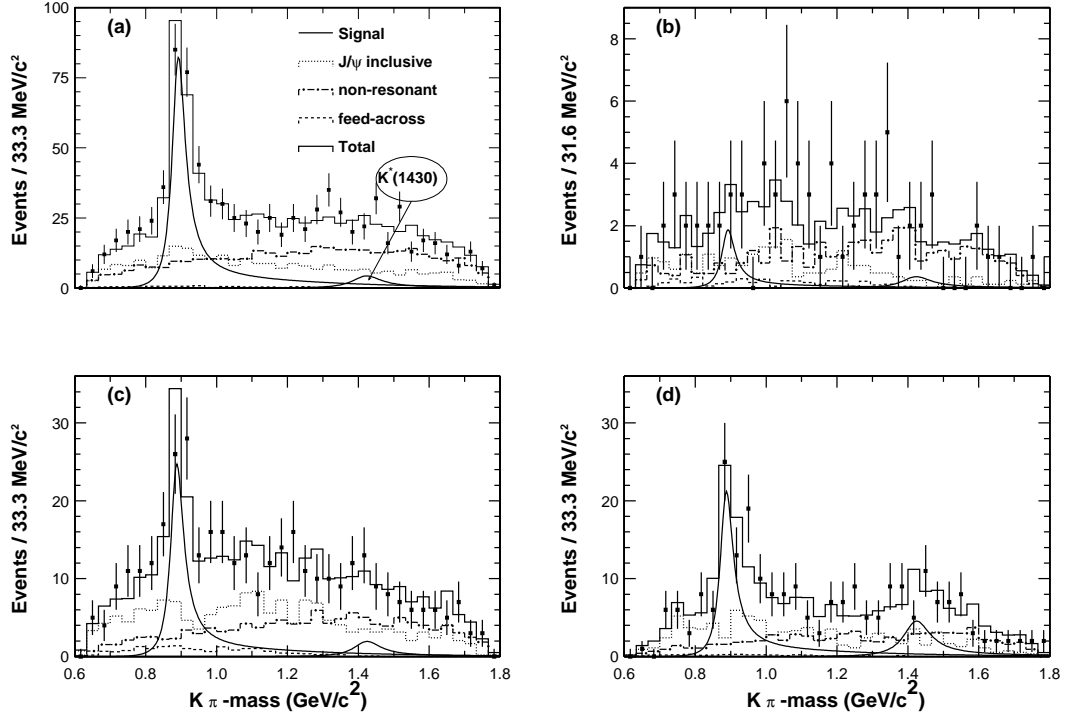


Fig. 3. The $K\pi$ -mass distribution for (a) $B^0 \rightarrow \chi_{c1} K^{*0} (K^+ \pi^-)$, (b) $B^0 \rightarrow \chi_{c1} K^{*0} (K_S^0 \pi^0)$, (c) $B^+ \rightarrow \chi_{c1} K^{*+} (K^+ \pi^0)$, and (d) $B^+ \rightarrow \chi_{c1} K^{*+} (K_S^0 \pi^+)$ decay modes, respectively, together with results from the fit to K^* signals and contributions of backgrounds due to J/ψ inclusive, non-resonant and feed-across backgrounds.

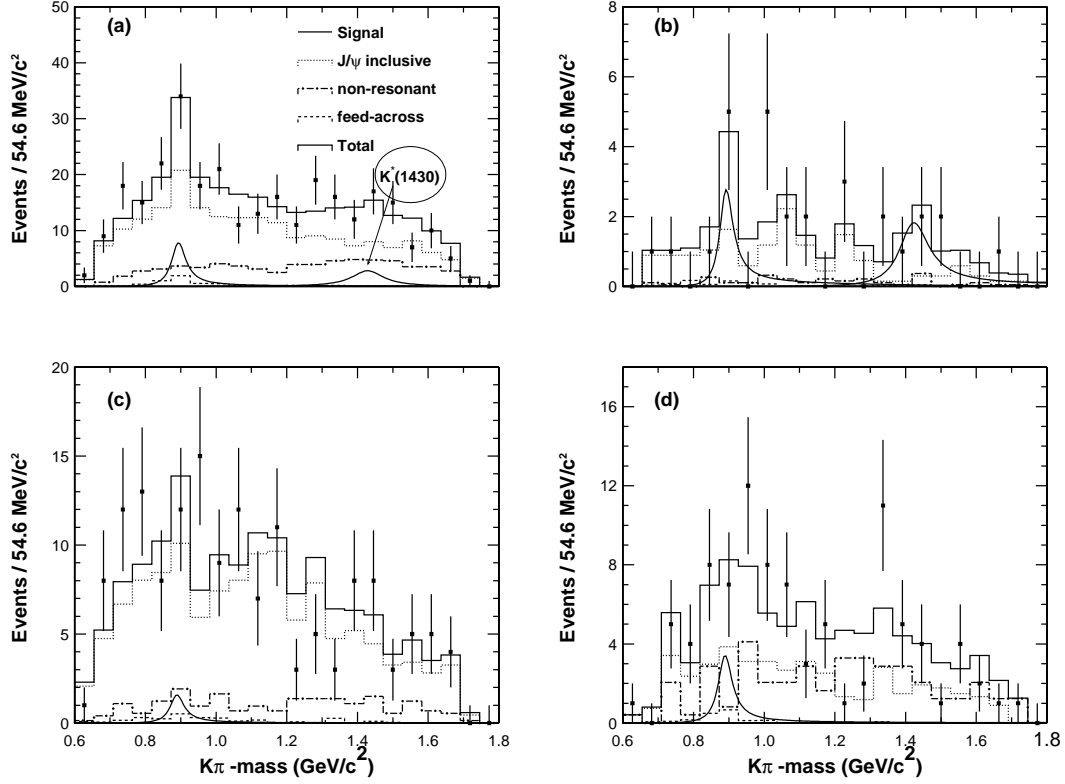


Fig. 4. The $K\pi$ -mass distribution for (a) $B^0 \rightarrow \chi_{c2}K^{*0}(K^+\pi^-)$, (b) $B^0 \rightarrow \chi_{c2}K^{*0}(K_S^0\pi^0)$, (c) $B^+ \rightarrow \chi_{c2}K^{*+}(K^+\pi^0)$, and (d) $B^+ \rightarrow \chi_{c2}K^{*+}(K_S^0\pi^+)$ decay modes, respectively, together with results from fit to K^* signals and contributions of backgrounds due to J/ψ inclusive, non-resonant and feed-across backgrounds.

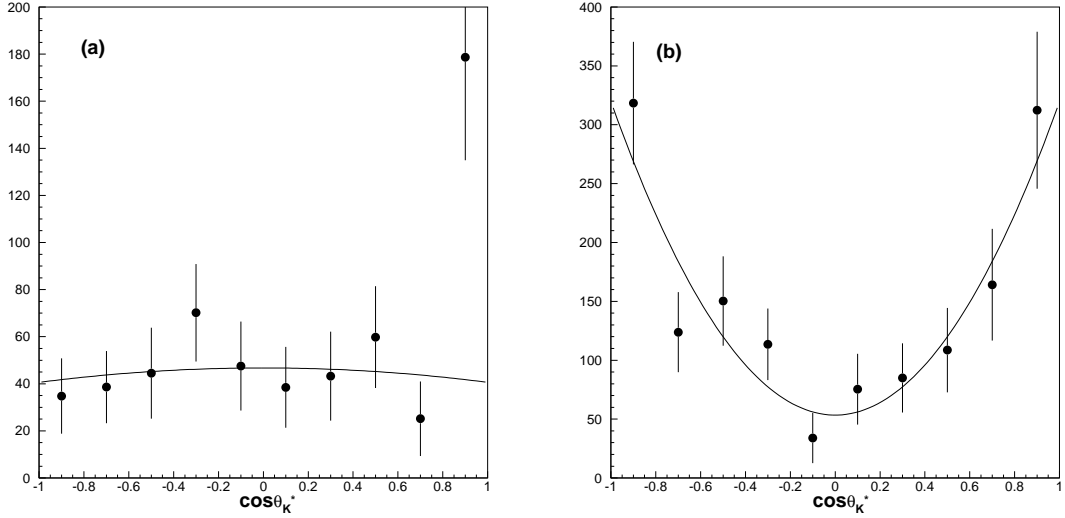


Fig. 5. The efficiency-corrected $\cos \theta_{K^*}$ distributions for $B^0 \rightarrow \chi_{c1}K^{*0}(K^+\pi^-)$ decay mode fitted with $F(\cos \theta_{K^*}) = A + 3B \cos^2 \theta_{K^*}$ function for (a) background region ($M_{K\pi} < 0.8 \text{ GeV}/c^2$) and (b) signal region ($0.821 \text{ GeV}/c^2 < M_{K\pi} < 0.971 \text{ GeV}/c^2$).

Table 1

The summary of the estimated branching fractions for $B \rightarrow \chi_{c1(2)}K(K^*)$ decay modes. The first (second) quoted error is statistical (systematic).

Mode	Efficiency $\mathcal{E}(\%)$	Yield	Br. Fraction (\mathcal{B}) $\times 10^{-4}$	U.L.(90% C.L.) $\times 10^{-4}$	Sign. (Σ)
$B^+ \rightarrow \chi_{c1}K^+$	25.4	645.7 ± 26.9	$4.49 \pm 0.19 \pm 0.53$		37.4
$B^0 \rightarrow \chi_{c1}K^0$	18.5	127.0 ± 11.8	$3.51 \pm 0.33 \pm 0.45$		15.3
$B^0 \rightarrow \chi_{c1}K^{*0}(K^+\pi^-)$	17.4	209.9 ± 22.7	$3.19 \pm 0.35 \pm 0.73$		12.1
$B^0 \rightarrow \chi_{c1}K^{*0}(K^0\pi^0)$	4.2	5.0 ± 4.8	$1.83 \pm 1.76 \pm 0.70$		1.1
$B^0 \rightarrow \chi_{c1}K^{*0}$			$3.14 \pm 0.34 \pm 0.72$		
$B^+ \rightarrow \chi_{c1}K^{*+}(K^0\pi^+)$	11.4	53.6 ± 11.1	$3.61 \pm 0.75 \pm 0.89$		6.9
$B^+ \rightarrow \chi_{c1}K^{*+}(K^+\pi^0)$	7.0	62.6 ± 13.2	$4.73 \pm 0.99 \pm 1.09$		6.0
$B^+ \rightarrow \chi_{c1}K^{*+}$			$4.05 \pm 0.59 \pm 0.95$		
$B^+ \rightarrow \chi_{c2}K^+$	24.9	14.8 ± 7.7	$0.16 \pm 0.08 \pm 0.02$	0.29	2.1
$B^0 \rightarrow \chi_{c2}K^0$	18.3	2.6 ± 2.1	$0.11 \pm 0.09 \pm 0.02$	0.26	1.6
$B^0 \rightarrow \chi_{c2}K^{*0}(K^+\pi^-)$	16.5	11.7 ± 9.4	$0.29 \pm 0.24 \pm 0.08$		1.3
$B^0 \rightarrow \chi_{c2}K^{*0}(K^0\pi^0)$	4.6	4.3 ± 3.5	$2.24 \pm 1.82 \pm 0.53$		1.6
$B^0 \rightarrow \chi_{c2}K^{*0}$			$0.32 \pm 0.23 \pm 0.08$	0.71	
$B^+ \rightarrow \chi_{c2}K^{*+}(K^0\pi^+)$	11.2	5.2 ± 5.4	$0.56 \pm 0.58 \pm 0.13$		1.1
$B^+ \rightarrow \chi_{c2}K^{*+}(K^+\pi^0)$	7.3	2.5 ± 7.2	$0.28 \pm 0.82 \pm 0.24$		0.3
$B^+ \rightarrow \chi_{c2}K^{*+}$			$0.47 \pm 0.47 \pm 0.13$	1.27	

Table 2

Summary of the multiplicative systematic errors in terms of percent (%) for all modes. Here the columns list the individual systematic error components: Trk., Lep. and Had. are those associated with tracking, lepton and hadron efficiencies; γ/π^0 refers to γ and π^0 reconstruction; K_S^0 refers to the K_S^0 selection efficiency; B.F. refers to the errors on secondary branching fractions; Inter. refers to the interference between K^* signal and non-resonant $K\pi$ background; Bkg. Shape refers to different background shapes used in studying interference; Ang. refers to the error due to the uncertainty of the angular distributions; Fit. Para. lists sensitivity to the fit parameters; Bkg. Errors refers to different fitting models for the J/ψ inclusive background; and Eff. Corr. lists errors associated with the efficiency correction.

Modes	Efficiency Uncertainty					B.F.	Inter.	Bkg. Shape	Ang.	Fit Para.($\pm 1\sigma$)	Bkg. Errors	Eff. Corr.	Total
	Trk.	Lep.	Had.	γ/π^0	K_S^0								
	%	%	%	%	%								
$B^+ \rightarrow \chi_{c1} K^+$	3.7	2.7	—	2	—	10.5	—	—	—	—	0.8	0.3	11.7
$B^0 \rightarrow \chi_{c1} K^0$	6.6	2.7	—	2	1	10.5	—	—	—	—	0.9	0.3	12.9
$B^0 \rightarrow \chi_{c1} K^{*0}(K^+\pi^-)$	5.2	2.7	1.9	2	—	10.5	15.0	10.8	5.1	—	2.0	0.3	22.9
$B^0 \rightarrow \chi_{c1} K^{*0}(K^0\pi^0)$	6.6	2.7	—	6	1	10.5	15.0	10.8	5.1	—	30.0	0.0	38.3
$B^+ \rightarrow \chi_{c1} K^{*+}(K^0\pi^+)$	8.1	2.7	0.8	2	1	10.5	15.0	10.8	5.1	—	7.0	0.4	24.6
$B^+ \rightarrow \chi_{c1} K^{*+}(K^+\pi^0)$	3.7	2.7	1.1	6	—	10.5	15.0	10.8	5.1	—	0.8	0.3	23.2
$B^+ \rightarrow \chi_{c2} K^+$	3.7	2.7	—	2	—	8.5	—	—	—	—	8.1	2.0	12.9
$B^0 \rightarrow \chi_{c2} K^0$	6.6	2.7	—	2	1	8.5	—	—	—	—	7.7	3.8	14.2
$B^0 \rightarrow \chi_{c2} K^{*0}(K^+\pi^-)$	5.2	2.7	1.9	2	—	8.5	15.0	10.8	5.1	—	15.4	1.7	26.9
$B^0 \rightarrow \chi_{c2} K^{*0}(K^0\pi^0)$	6.6	2.7	—	6	1	8.5	15.0	10.8	5.1	—	4.7	2.3	23.6
$B^+ \rightarrow \chi_{c2} K^{*+}(K^0\pi^+)$	8.1	2.7	0.8	2	1	8.5	15.0	10.8	5.1	3.8	1.9	1.9	23.2
$B^+ \rightarrow \chi_{c2} K^{*+}(K^+\pi^0)$	3.7	2.7	1.1	6	—	8.5	15.0	10.8	5.1	8.0	84.0	4.0	87.4

Table 3

Comparison between this measurement and those at BaBar [21,22]. The first (second) quoted error is statistical (systematic).

Mode	Belle		BaBar	
	Br. Fraction $\times 10^{-4}$	U.L.(90% C.L.) $\times 10^{-4}$	Br. Fraction $\times 10^{-4}$	U.L.(90% C.L.) $\times 10^{-4}$
$B^+ \rightarrow \chi_{c1} K^+$	$4.49 \pm 0.19 \pm 0.53$		$5.79 \pm 0.26 \pm 0.65$	
$B^0 \rightarrow \chi_{c1} K^0$	$3.51 \pm 0.33 \pm 0.45$		$4.53 \pm 0.41 \pm 0.51$	
$B^0 \rightarrow \chi_{c1} K^{*0}$	$3.14 \pm 0.34 \pm 0.72$		$3.27 \pm 0.42 \pm 0.64$	
$B^+ \rightarrow \chi_{c1} K^{*+}$	$4.05 \pm 0.59 \pm 0.95$		$2.94 \pm 0.95 \pm 0.98$	
$B^+ \rightarrow \chi_{c2} K^+$	$0.16 \pm 0.08 \pm 0.02$	0.29	$0.09 \pm 0.10 \pm 0.11$	0.30
$B^0 \rightarrow \chi_{c2} K^0$	$0.11 \pm 0.09 \pm 0.02$	0.26	$0.21 \pm 0.11 \pm 0.13$	0.41
$B^0 \rightarrow \chi_{c2} K^{*0}$	$0.32 \pm 0.23 \pm 0.08$	0.71	$0.14 \pm 0.11 \pm 0.14$	0.36
$B^+ \rightarrow \chi_{c2} K^{*+}$	$0.47 \pm 0.47 \pm 0.13$	1.27	$-0.15 \pm 0.05 \pm 0.14$	0.12